DTU Library

Real-time monitoring and optimization of a large-scale heat pump prone to fouling - towards a digital twin framework

Aguilera, José Joaquín; Meesenburg, Wiebke; Markussen, Wiebke Brix; Zühlsdorf, Benjamin; Elmegaard, Brian

Published in:
Applied Energy

Link to article, DOI:
10.1016/j.apenergy.2024.123274

Publication date:
2024

Document Version
Publisher's PDF, also known as Version of record

Applied Energy 365 (2024) 123274

Contents lists available at ScienceDirect

Applied Energy

journal homepage: www.elsevier.com/locate/apenergy

Real-time monitoring and optimization of a large-scale heat pump prone to fouling - towards a digital twin framework

José Joaquín Aguilera [a,*], Wiebke Meesenburg [a], Wiebke Brix Markussen [b], Benjamin Zühlsdorf [b], Brian Elmegaard [a]

[a] Section of Thermal Energy, Department of Civil and Mechanical Engineering, Technical University of Denmark, Nils Koppels Alle 403, Kgs. Lyngby 2800, Denmark
[b] Danish Technological Institute, Kongsvang Allé 29, Aarhus C 8000, Denmark

HIGHLIGHTS

- Use of a model calibrated online to simulate a two-stage ammonia heat pump.
- Online calibration enabled to assess fouling growth and mitigation in real-time.
- Intermediate pressure set points were optimized through the online calibrated model.
- Online calibration improved performance estimations by 3 to 17 percentage points.
- Model-based fouling monitoring was beneficial for the set point optimization.

ARTICLE INFO

Keywords:
Digital twin
Set point optimization
Performance degradation
Fault-tolerant control
Fault diagnosis

ABSTRACT

Large-scale heat pumps are a promising technology for the decarbonisation of heat supplied in buildings and industries, provided they operate as expected. However, common faults like fouling and unplanned downtime periods can significantly affect their performance and availability. This could limit the widespread adoption of large-scale heat pumps over other heating technologies such as gas and electric boilers. Approaches described in the literature to optimize the operation of large-scale heat pumps often lack validation under real-world conditions and do not account for performance degradation due to faults. This work demonstrates a step towards utilizing digital twins to improve the energy performance of a commercial large-scale heat pump affected by fouling. A framework was proposed based on the real-time adaptation of digital twins, where a simulation model was calibrated online based on measurements from the heat pump in operation, which was then used for set point optimization. This enabled to determine optimal intermediate pressure set points in the heat pump operating under varying levels of fouling over time. The framework was tested on different periods of heat pump operation spread over ten calendar months. The results showed that the use of online calibration rather than a single calibration decreased performance estimation errors between 3 and 17 percentage points. Moreover, the set points determined by the online-calibrated model, along with a simpler polynomial model derived from it, showed improvements in the heat pump performance by up to 3%, depending on the level of fouling. The findings of this study demonstrated the potential to extend the proposed framework using digital twins to enhance the energy efficiency of large-scale heat pumps.

1. Introduction

Large-scale heat pumps can be utilized for recovering industrial excess heat and harnessing natural heat sources to supply district heating in densely populated areas [1]. The EU Energy Roadmap [2] indicated that district heating has the potential to fulfil around half of the heating demand in European households, and the adoption of large-scale heat pumps could contribute to approximately 25% to 30% of this capacity. Moreover, electricity-driven mechanical compression heat pumps enable the integration of the heating and electricity sectors while simultaneously reducing cooling and heating costs, making them an attractive technology for the decarbonisation of the industrial sector [3].

Given the key role that large-scale heat pumps are expected to have

* Corresponding author.
E-mail address: jojap@mek.dtu.dk (J.J. Aguilera).

https://doi.org/10.1016/j.apenergy.2024.123274
Received 6 December 2023; Received in revised form 3 April 2024; Accepted 17 April 2024
Available online 25 April 2024

Abbreviations

AM	adaptive model
API	application programming interface
CF	correction factor
CIP	cleaning-in-place
FM	fixed model
GM	geometric average
HEX	heat exchanger
HMI	human-machine interface
HS	high-stage
LS	low-stage
(N)RMSE	(normalized) root mean square error
res	residual
SCADA	supervisory control and data acquisition
SM	surrogate model

Letter symbols

A	heat transfer area, m^2
Cp	specific heat capacity, kJ/kgK
dp	pressure difference, bar
dT	temperature difference, K
$\dot{m}$	mass flow rate, kg/s
N	compressor speed, rpm
$\dot{Q}$	heat flow rate, kW
p	pressure, bar
R	thermal resistance, K/kW
T	temperature, °C
U	overall heat transfer coefficient, kW/Km^2
V	volume, m^3
$\dot{V}$	volume flow rate, m^3/s
w	weight, –
$\dot{W}$	power, kW

Greek symbols

ρ	density, kg/m^3
η	efficiency, –

Subscripts and superscripts

c	condensation
calc	calculated
clean	clean
con	condenser
DSH	desuperheater
meas	measurement
e	evaporation
eva	evaporator
f	fouling
IC	Intercooler
in	inlet
is	isentropic
m	intermediate
opt	optimal
out	outlet
pp	pinch-point
ref	refrigerant
s	swept
SC	sub-cooler
sim	simulation
sink	sink stream
sp	set point
source	source stream
total	total
th	thermal
vol	volumetric
w	water

in the decarbonisation of energy systems, their rate of installation is expected to increase over the next decade. As described in [1], countries like Finland, Austria, Sweden, and Denmark have set targets to achieve net-zero emissions from their district heating systems between 2030 and 2040, where extending the adoption of large-scale heat pumps will become increasingly relevant. For instance, Denmark aims to reach this target by producing approximately one-third of its total district heat supply through large-scale heat pumps by 2030 [4]. As of 2023, the number of heat pumps installed in Danish district heating systems has more than tripled compared to the year 2019 [5].

Large-scale heat pumps will be relevant for the decarbonisation of the building and industrial sectors, provided that they meet expected levels of availability and performance. Compared to heat pumps used in households and other smaller applications, large-scale heat pumps have higher reliability requirements due to a larger number of components, increased economic impact of downtime, and a larger number of end-users. Moreover, large-scale heat pumps can be affected by operational challenges such as specific faults on the heat source that are not present in other mechanical vapour compression systems, as highlighted in [6]. Therefore, the use of dedicated services for a growing number of large-scale heat pumps will be crucial for ensuring their reliable operation in future energy systems.

1.1. Fouling in large-scale heat pumps

Large-scale heat pumps are affected by faults related to the heat source the use, which can increase their operational costs and limit their broader adoption. Among faults affecting the operation of large-scale heat pumps, fouling on the source side of heat exchangers was described in the literature as the most frequent fault [6]. Fouling is regarded as the deposition of material on heat transfer surfaces that may lead to the degradation of performance in heat pumps. Fouling may also lead to a significant increase in operational and maintenance costs, as well as downtime periods given that mitigation strategies often require a shutdown of the system [7]. Pogiatzis et al. [8] indicated that inadequate planning of fouling mitigation processes, like cleaning heat exchangers and replacing filters, can accelerate the aging of heat exchangers and reduce the efficacy of future mitigation strategies.

The prediction of fouling-related effects in heat pumps is often challenging since the instant in which the first deposition occurs and its growth rate over time require detailed numerical models and experimental measurements [9]. Pelet and Favrat [10] identified fouling in a lake-water source heat pump by the analysis of gradual changes in the pinch-point temperature difference in the evaporator. Gjengedal et al. [11] characterized fouling in a ground source heat pump using a step-test procedure. This method decoupled the influence of fouling on the source stream pressure drop from variations caused by a variable-speed pump. Borges et al. [12] applied a model based on artificial neural networks for the prediction of the performance of a heat pump under the influence of evaporator fouling. In their study, a dynamic simulation model was used to emulate the effects of fouling in the heat pump. This was used for the development and testing of their data-driven model. Meesenburg et al. [13] employed measured data, a basic physics-based model and data-driven forecasting to predict fouling growth in a large-scale heat pump. These results were used for estimating the performance of the heat pump through dynamic simulation. Their findings indicated that fouling raised the thermal resistance of the source heat exchanger of the heat pump by 68%, resulting in a 4% decrease in its COP of around

4.5.

1.2. Optimization of two-stage systems

In addition to addressing frequent faults in large-scale heat pumps, optimizing the energy performance of these systems can enhance their widespread adoption over other heating technologies such as gas and electric boilers. The optimization of heat pump systems in terms of the first law of thermodynamics involves maximizing the heat removal rate for the minimum power input. In particular, off-design optimization of heat pumps offers the possibility to reduce their energy consumption and operational costs.

Two-stage compression and two-stage throttling is a widely utilized configuration in large-scale heat pumps, particularly in applications where ammonia is used as a working fluid. This configuration requires finding an optimum intermediate pressure for the efficient operation of the heat pump. A commonly used approximation of the optimal intermediate pressure for two-stage systems is the geometric average between the condensation and evaporation pressures. Tiedeman et al. [14] found that using the geometric average led to deviations with the optimum intermediate pressure in ammonia systems by up to 26%. The authors applied an approximation of the optimal intermediate pressure that included compressor efficiencies and the second-law efficiency of the cycle. This approximation led to estimations of the coefficient of performance (COP) that were within 2% from the optimal COP.

Previous studies proposed methods for determining the optimal intermediate pressure of a particular system by the use of its operational data. Wang et al. [15] and Gong et al. [16] optimized the intermediate pressure set point by means of a model-free approach named extremum seeking control. Their framework was tested in dynamic simulation models, where the total power consumption was minimized by controlling the upper expansion valve in accordance with a calculated intermediate pressure set point. The simulation results by Wang et al. demonstrated an approximately 5% rise in the COP, from 2.1 to 2.2, when supplying approximately 10 kW of heat, compared to using a fixed set point. Similarly, Gong et al. observed around an 8% increase in COP, from 2.2 to 2.6, in contrast to a fixed set point in a heat pump with a heat output of 200 kW. However, it remains unclear how the fixed set points utilized as benchmarks were determined in both studies by Wong et al. and Gong et al.

1.3. Adaptive simulation models

Set point optimization frameworks found in the literature often consider the operation of heat pump and refrigeration systems under fault-free conditions. To the best of the authors ́knowledge, none of the studies present in the literature applied set point optimization for heat pump systems affected by performance degradation due to faults.

Advances in modelling tools for simulating the operation of large-scale heat pumps may lead to improved monitoring and control strategies. Simulation models mainly based on thermodynamics enable the representation of the operation of heat pumps under a wide variety of boundary conditions. However, the parameters used in those models are often fixed and given by characteristics defined during the design of the system. This may limit the ability of thermodynamic simulation models to describe accurately the operation of heat pumps affected by performance degradation, particularly when exposed to faults and aging of components.

Modern communication and information technologies enable to retrieve and process operational data in real-time. This has led to the development of simulation models that can adjust at least part of their structure based on observations from the physical system they represent, also referred to as digital twins. As indicated in [17], digital twin frameworks have a bi-directional communication between the model and the physical system. However, previous studies also used the concept of digital twins in frameworks with a one-directional flow of information from the physical system to the model. Applications where digital twins have been used include manufacturing processes [18,19] and energy systems [20–23]. Moreover, a number of studies proposed digital twin-based services for refrigeration and heat pump systems. Examples of this include performance monitoring [24], predictive maintenance [25,26], and operation optimization [27,28]. However, the use of digital twins in the heat pump industry remains limited.

1.4. Scope of the study

The present study aims at increasing the energy performance of a large-scale heat pump prone to fouling in real-time through a model-based framework for performance degradation monitoring and set point optimization. Operational data was retrieved remotely from a commercial large-scale heat pump used as a case study, which was used for the development and testing of the proposed framework.

This paper is structured as follows: The description of the case study, data processing, simulation model, and calibration process are included in Section 2. Section 3 contains the simulation results and their validation based on measured data, as well as the results from the set point optimization process. The results and limitations of the study are discussed in Section 4. Finally, the main conclusions are included in Section 5.

2. Method

The overall structure of the monitoring and optimization framework from this study is shown in Fig. 1. The heat pump used as a case study is operated and controlled through a wired supervisory and control system that applies the communication protocol Profibus-DP. This system retrieves data from actuators and sensing devices, which are stored and displayed in a local supervisory control and data acquisition (SCADA) system. As reported in [29], SCADA systems are often used in large-scale heat pump systems, where operational data is stored in a local server. The SCADA system in the case study heat pump was connected with the cloud computing platform from Microsoft, called Azure. This setup is becoming increasingly popular in large SCADA systems because it allows the remote availability and storage of large amounts of operational data [30]. In the setup shown in Fig. 1, the operational data was retrieved with Python through an application programming interface (API). This scheme only allows the transfer of data from the SCADA system to the API and not vice versa, which prevents the remote manipulation of the local controllers of the heat pump for security reasons.

The setup shown was applied for the provision of performance and fouling monitoring as well as set point optimization. Here, relevant information derived from adaptive simulation models was displayed to the human operator through a human-machine interface (HMI). This information included the current status of the heat pump in terms of performance indicators, the possibility to improve such indicators through the adjustment of control set points and the level of performance degradation. Given that the information flow between the heat pump and the model was not bi-directional, the proposed framework requires to be extended to be completely regarded as a digital twin framework. This extension may include the automatic adjustment of set points in the heat pump controllers rather than requiring humans to do this task.

2.1. Case study heat pump

The heat pump assessed in the present study was a two-stage ammonia heat pump located in Copenhagen, Denmark. This heat pump has a designed heating capacity of 2 MW and supplies heat to a district heating network at approximately 68 °C. It uses industrial wastewater from a biochemical production plant at around 25 °C as the heat source, which is required to be cooled down to 18 °C to be rejected to the sewage system. A diagram of the heat pump layout is shown in

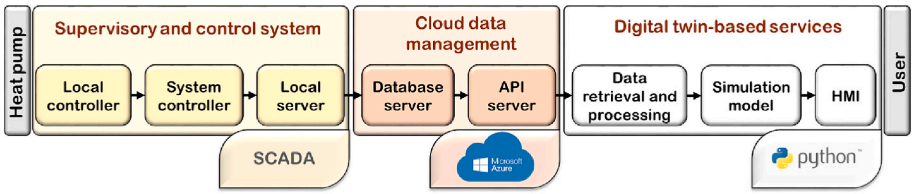

Fig. 1. Flow diagram of the main components used for the provision of digital twin-based services.

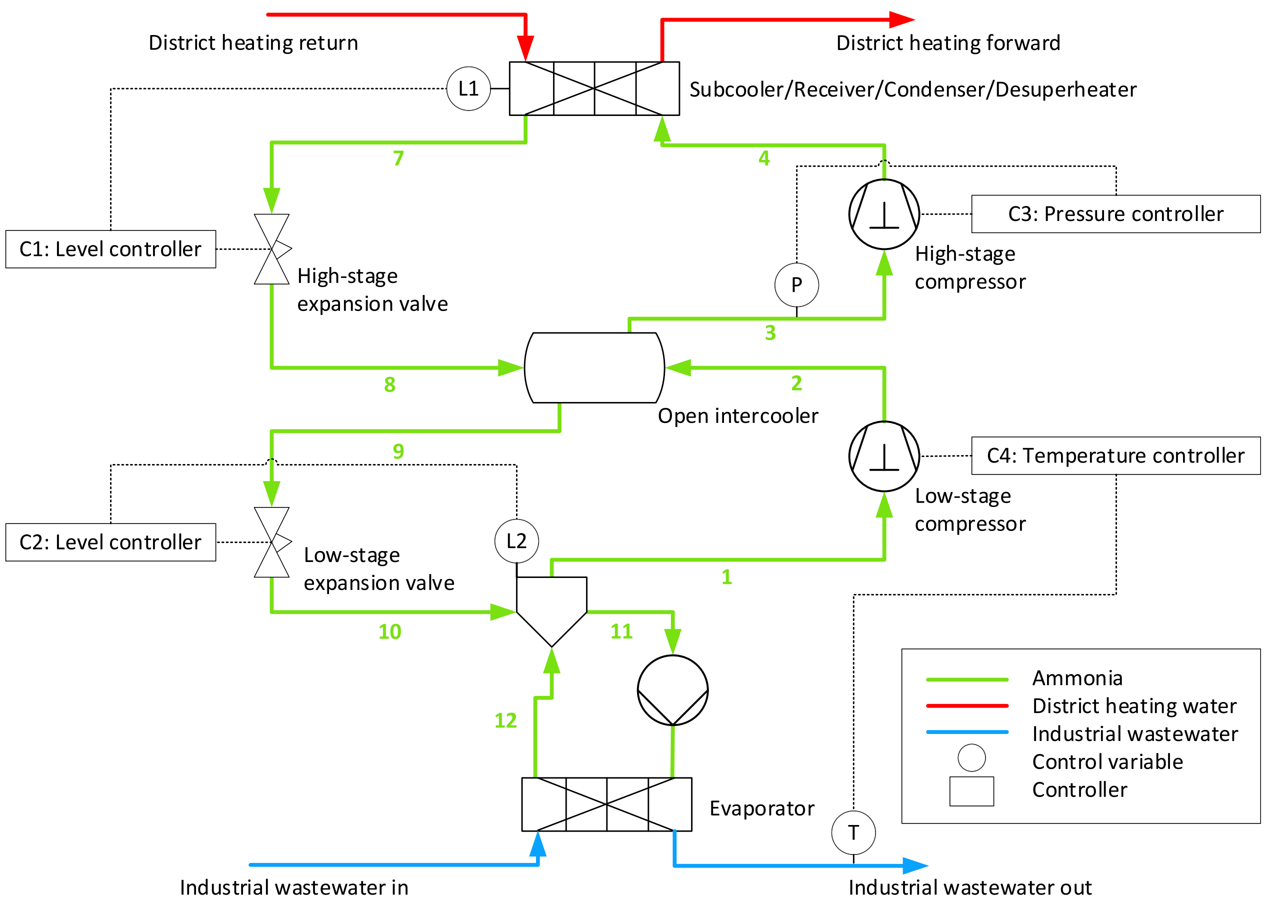

Fig. 2. Layout of the two-stage ammonia heat pump analyzed in the present study.

Fig. 2.

The main components of the heat pump include two different reciprocating compressors for the high and low stages, a shell-and-plate evaporator, an open intercooler between both stages, electronic expansion valves for each of the two stages, and a single shell-and-plate heat exchanger that comprises a desuperheater (DSH), condenser, receiver, and sub-cooler.

The heat pump is controlled by four controller units shown in Fig. 2. In the low stage, a controller regulates the speed of the compressor based on the water temperature at the evaporator outlet, whereas the opening degree of the expansion valve is controlled by the filling level of refrigerant in the evaporator. In the high stage, the opening degree of the expansion valve depends on the filling level of refrigerant inside the receiver embedded into the condenser unit. The speed of the high-stage compressor is adjusted based on the intermediate pressure. Capacity control is achieved by the adjustment of the low-stage compressor speed given variations in the water temperature at the evaporator outlet. Consecutively, this leads to the adjustment of the high-stage compressor speed resulting from a variation of the intermediate pressure.

The evaporator is in direct contact with the industrial wastewater used as the heat source, resulting in the presence of fouling on the source side. The evaporator cannot be opened and thereby its interior cannot be directly accessed for cleaning. The removal of fouled material is done through a chemical cleaning-in-place (CIP) system, which requires the heat pump to be shut down. Two types of CIPs have been tested in the heat pump, namely a two-day CIP that uses a single cleaning agent and a three-day CIP where two cleaning agents are used, one after the other. These agents are an acid and a basic chemical solution for the removal of inorganic and organic depositions, respectively. The decision on the type of CIP used and how frequently it is applied is taken by the heat pump operator based on their own experience.

2.2. *Data retrieval and processing*

The operational data from the heat pump was retrieved at a one-minute interval from the cloud data management system through the API, as shown in Fig. *1*. The retrieval and processing of data are done through Python. Table 1 shows the operational parameters from the heat pump that were retrieved from the SCADA server. Such parameters were used to calibrate a simulation model of the heat pump, presented in

Table 1
Retrieved parameters from the SCADA server related to the operation of the heat pump.

Retrieved parameter from SCADA		Symbol	Unit
Physical quantity	Measurement location		
Water temperature	Subcooler inlet	$T_{sink,in}$	°C
	Desuperheater outlet	$T_{sink,out}$	°C
	Evaporator inlet	$T_{source,in}$	°C
	Evaporator outlet	$T_{source,out}$	°C
Water volume flow rate	Subcooler inlet	V_{sink}	m^3/h
	Evaporator inlet	V_{source}	m^3/h
Water pressure (gauge)	Evaporator inlet	$p_{source,in}$	bar
	Evaporator outlet	$p_{source,out}$	bar
Ammonia temperature	Low-stage compressor inlet	$T_{suc,LS}$	°C
	Low-stage compressor outlet	$T_{dis,LS}$	°C
	High-stage compressor inlet	$T_{suc,HS}$	°C
	High-stage compressor outlet	$T_{dis,HS}$	°C
	Condenser outlet	T_c	°C
	Evaporator inlet	T_e	°C
Ammonia pressure (gauge)	Low-stage compressor inlet	$p_{suc,LS}$	bar
	Low-stage compressor outlet	$p_{dis,LS}$	bar
	High-stage compressor inlet	$p_{suc,HS}$	bar
	High-stage compressor outlet	$p_{dis,HS}$	bar
Power intake	Low-stage compressor	$\dot{W}_{LS}$	kW
	High-stage compressor	$\dot{W}_{HS}$	kW

Section 2.3. An example of the time-series data collected from the heat pump is shown in Fig. 11, included in Appendix A.

All the refrigerant states in the cycle were calculated with the Coolprop database [31]. This required determining the mass and energy balances in all the relevant components of the heat pump. The heat output of the heat pump and its COP were calculated based on Eq. (1) and Eq. (2), respectively. This required the knowledge on the mass flow rate of water in the sink stream ($\dot{m}_{sink}$), the specific heat of water ($c_{p,w}$), the return and forward temperatures of water to the district heating network ($T_{sink,in}$ and $T_{sink,out}$, respectively), as well as the sum of the power intake from the low and high stage compressors ($\dot{W}_{total}$).

$$\dot{Q}_{sink} = c_{p,w} \bullet \dot{m}_{sink} \bullet \left(T_{sink,out} - T_{sink,in}\right) \tag{1}$$

$$\mathrm{COP} = \dot{Q}_{sink} \Big/ \dot{W}_{total} \tag{2}$$

2.3. Simulation model

A comparison was made between a simulation model that was adjusted based on an initial calibration with and without accounting for changes in fouling-related parameters, which were named adaptive and fixed models, respectively. This aimed at assessing the extent by which the adaptive model could outperform the fixed model in terms of correspondence between simulated and measured data.

The adaptive and fixed models were based on the same simulation model of the case study heat pump. This was a quasi-steady-state model that was built in Python. The model used six parameters as inputs that were external to the heat pump, namely the temperatures of water at the inlet and outlet of the evaporator ($T_{source,in}$ and $T_{source,out}$, respectively), the temperature of water at the inlet of the condenser ($T_{sink,in}$), the volumetric flow rates in the source and sink streams (V_{source} and V_{sink}, respectively) and the set point for the intermediate pressure ($p_{m,sp}$). The internal input parameters of the model were the overall heat transfer coefficients (U) and heat transfer areas (A) of all heat exchangers, the temperature difference at the pinch point of the condenser ($dT_{pp,cond}$), the isentropic and volumetric efficiencies of the compressors (η_{is} and η_{vol}, respectively) as well as their swept volumes (V_s). Additionally, the internal input parameters included the effects of fouling on the evaporator thermal resistance ($R_{th,f}$) and source pressure drop ($dp_{source,f}$). These two parameters as well as the heat transfer coefficients were calibrated based on measurements as described in Section 2.4.

The model used two iteration routines, shown in Fig. 3. These two routines were used rather than only one because they solved two different numerical problems, namely a root finding and an optimization problem. The inner routine solved the root finding problem, where it determined all the refrigerant states in the cycle by the use of the Coolprop database [31] as well as mass and energy balances over each component. This resulted in a system of equations that was solved by an algorithm that applied the Newton-Raphson method. In this routine, the iteration variables were the condensation pressure (p_c), intermediate pressure (p_m), and the speed of the low-stage compressor (N_{LS}). The outer routine solved an optimization problem by determining the speed of the high-stage compressor (N_{HS}) which led to the minimum difference between the intermediate pressure and its set point. This was solved by a minimization algorithm based on the least-squares method available from the Python module SciPy [32].

The compressors were assumed adiabatic. The volumetric and isentropic efficiencies of the compressors were represented by polynomial regression models. These regression models were fitted and validated based on design data obtained from the compressor manufacturer. The input variables for the regression models were the pressure ratio, the refrigerant state at the inlet, and the compressor speed. The fitting process was based on the least squares method and applied the refrigerant states at the inlet and outlet of the compressors as well as their rotational speed.

The heat transferred in each of the heat exchangers in the model (i.e. DSH, condenser, SC, and evaporator) was represented by Eq. (3), Eq. (4), and Eq. (5). The UA-values were determined from the design specifications provided by the heat pump manufacturer. These UA-values were assumed to be invariable as a result of varying mass flow rates. The pressure drop on the refrigerant side was neglected in all heat exchangers. The pressure drop on the secondary side was calculated only for the evaporator, whereas it was neglected for the other heat exchangers. The reason for this was that magnitude of the pressure drop in the source stream were expected to be influenced by fouling, which was within the scope of analysis in the present study. The pressure drop on the source side of the evaporator (dp_{source}) was determined based on a quadratic regression model that depended on the mass flow rate of water.

$$\dot{Q}_{HEX} = c_{p,w} \bullet \dot{m}_w \bullet \left(T_{w,out} - T_{w,in}\right) \tag{3}$$

$$\dot{Q}_{HEX} = \dot{m}_{ref} \bullet \left(h_{ref,out} - h_{ref,in}\right) \tag{4}$$

$$\dot{Q}_{HEX} = \mathrm{UA}_{HEX} \bullet \mathrm{LMTD}_{HEX} \tag{5}$$

The Q_{HEX} was the heat exchanged in each heat exchanger; $\dot{m}_{ref}$ and $\dot{m}_w$ were the mass flow rates of refrigerant and water, respectively; $T_{w,in}$ and $T_{w,out}$ were the inlet and outlet temperatures of water, respectively; $h_{ref,in}$ and $h_{ref,out}$ were the inlet and outlet specific enthalpies of the refrigerant; and LMTD_{HEX} was the logarithmic mean temperature difference in each heat exchanger, described in [33].

Table 2 summarizes all the time-invariant input parameters included in the heat pump model. This does not include the speed of the compressors, since they were calculated for each simulation interval. The speed of the compressors were bounded between 700 rpm and 1800 rpm, which was an interval specified by the manufacturer.

The effects of fouling on the evaporator were described by Eq. (6) and Eq. (7). This required determining the thermal resistance and source pressure drop of the heat pump operating under fouling-free conditions ($R_{th,clean}$ and $dp_{source,clean}$, respectively). $R_{th,clean}$ was calculated from the

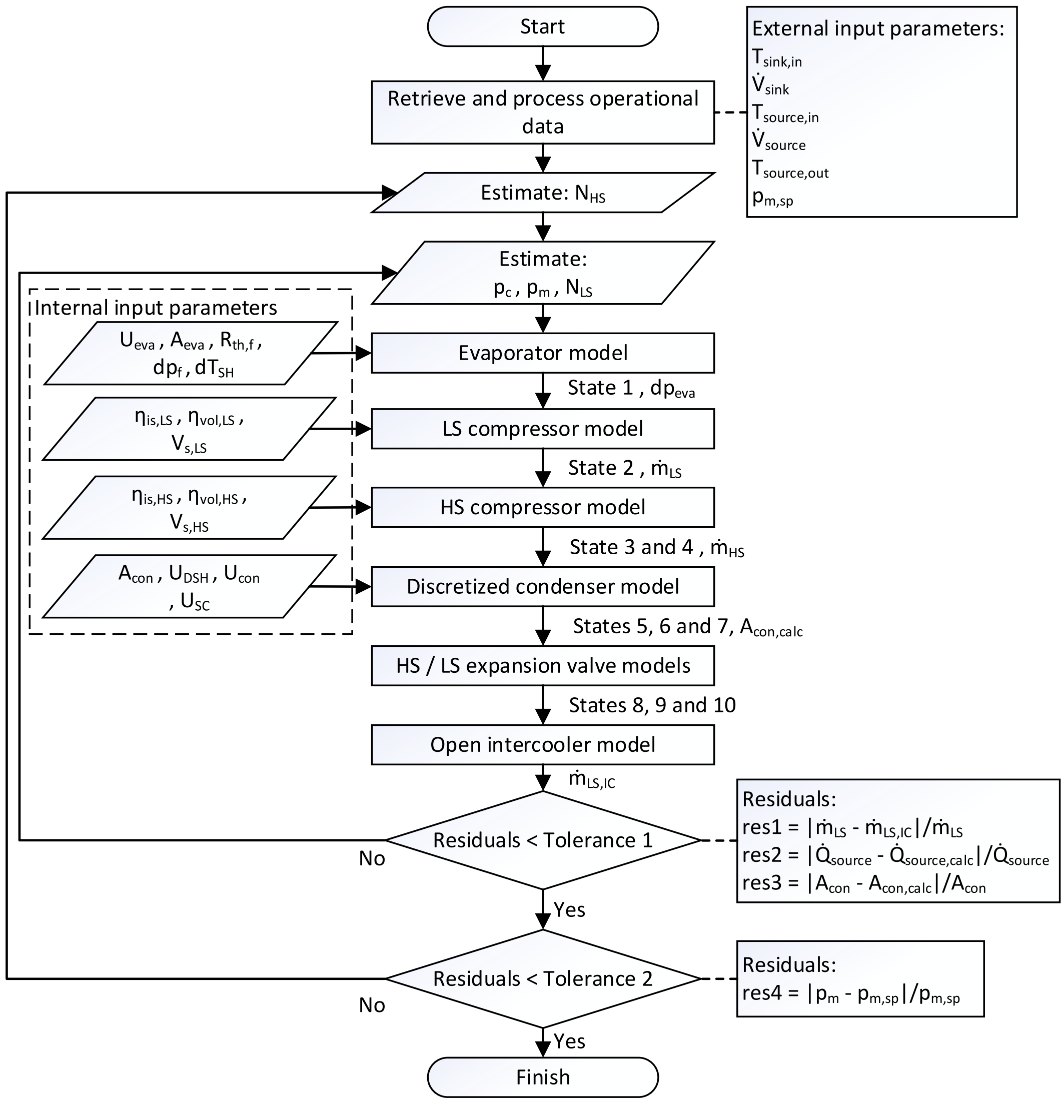

Fig. 3. Flowchart of the quasi-steady-state simulation model.

Table 2
Input parameters used in the different components of the simulation model.

Component	Input parameter	Symbol	Value	Unit
DSH	Overall heat transfer coefficient	U_{DSH}	230	W/m^{2}K
	Heat transfer area	A_{DSH}	27.8	m^2
Condenser	Overall heat transfer coefficient	U_{con}	1210	W/m^{2}K
	Heat transfer area	A_{con}	100.6	m^2
SC	Overall heat transfer coefficient	U_{SC}	452	W/m^{2}K
	Heat transfer area	A_{SC}	23.1	m^2
Evaporator	Overall heat transfer coefficient	U_{eva}	3000	W/m^{2}K
	Heat transfer area	A_{eva}	91.96	m^2
	LS suction superheat	dT_{SH}	1	K
Low-stage compressor	Swept volume	$V_{s,LS}$	1018	m^3/rev
High-stage compressor	Swept volume	$V_{s,HS}$	532	m^3/rev

design evaporator heat transfer coefficient shown in Table 2, whereas its correction factor (CF_{eva}) was adjusted once using operational data, as described in Section 2.4. $R_{th,f}$ and the correction factor for the source pressure drop ($CF_{dp,f}$) were included as time-dependent input parameters in the model (seen in Fig. 3) and were calibrated online.

$$R_{th,f} = 1/UA_{eva} - 1/\left(CF_{eva} \bullet UA_{eva,clean}\right) = R_{th} - R_{th,clean} \tag{6}$$

$$dp_{source} = dp_{source,f} + dp_{source,clean} = CF_{dp,f} \bullet dp_{source,clean} \tag{7}$$

2.4. Model calibration

Model calibration is defined by Trucano et al. [34] as the process in which parameters inside a model are adjusted in order to maximize the agreement between simulated and measured data. In the present study, the variables analyzed during a calibration process were named calibration targets, whereas the internal model parameters adjusted during this process were defined as calibration parameters. The normalized root mean square error (NRMSE) was used to evaluate the correspondence between simulated and measured calibration targets. The aim of a calibration process was to minimize the NRMSE between calibration targets over a time period n, represented by Eq. (8) and Eq. (9). Here, the level of importance of a particular calibration target was described by its weight factor (w). The calibration parameters that led to the minimum NRMSE between calibration targets were obtained through a quasi-Newton optimization algorithm available in the SciPy module from Python [32].

$$minf(\text{Parameter}) = \sum_{i=1}^{n} w_i \bullet \text{NRMSE}_i \quad (8)$$

$$\text{NRMSE}_i = \overline{\text{Target}_{\text{meas}}}^{-1} \bullet \sqrt{n^{-1}\sum_{i=1}^{n}\left(\text{Target}_{\text{sim},i}(\text{Parameter}) - \text{Target}_{\text{meas},i}\right)^2} \quad (9)$$

Fig. 4 shows the two types of calibration processes used in this study, namely the initial calibration and fouling calibration. In the initial calibration, the UA-values of all heat exchangers in the model were adjusted through correction factors (CF). These were considered time-invariant calibration parameters. The targets of the initial calibration were $\dot{Q}_{\text{sink}}$, $\dot{W}_{\text{total}}$, and the evaporation pressure (p_e), each of which had weights $w = 0.33$ (i.e. equally weighted). The data used for the initial calibration was operational data retrieved during the site acceptance test of the heat pump. This test was performed right after the heat pump was installed and thereby the influence of fouling on the heat pump was considered negligible.

In the fouling calibration, time-dependent parameters were adjusted. These parameters were related to the effects of fouling on the performance degradation of the heat pump, namely $R_{\text{th,f}}$ and $\text{CF}_{\text{dp,f}}$. The target variables used in the fouling calibration were p_e and dp_{source}, both weighted equally with $w = 0.5$. These variables were selected since they were directly affected by the increased thermal resistance and pressure drop due to fouling. The operational periods for the fouling calibration process were not selected automatically, but were defined directly by the user of the monitoring and optimization framework. In this study, such periods were representative operational periods of the heat pump at full load and part load operation given different levels of fouling, as described in Section 2.6.

A summary of the parameters adjusted in the initial calibration and fouling calibration processes is shown in Table 3. Here, the limits for each of the calibrated parameters and the start values for the calibration processes were defined heuristically based on the experience obtained

Table 3
Parameters adjusted in the initial calibration and fouling calibration processes, including their start values and limits for the calibration.

Calibration process	Calibration parameter	Start value	Lower limit	Upper limit	Unit
Initial	CF_{DSH}	1	0.5	2	(–)
	CF_{con}	1	0.5	2	(–)
	CF_{SC}	1	0.5	2	(–)
	CF_{eva}	1	0.5	2	(–)
Fouling	$R_{\text{th,f}}$	0	0	$8\bullet10^{-3}$	(K/kW)
	$\text{CF}_{dp,f}$	1	1	2	(–)

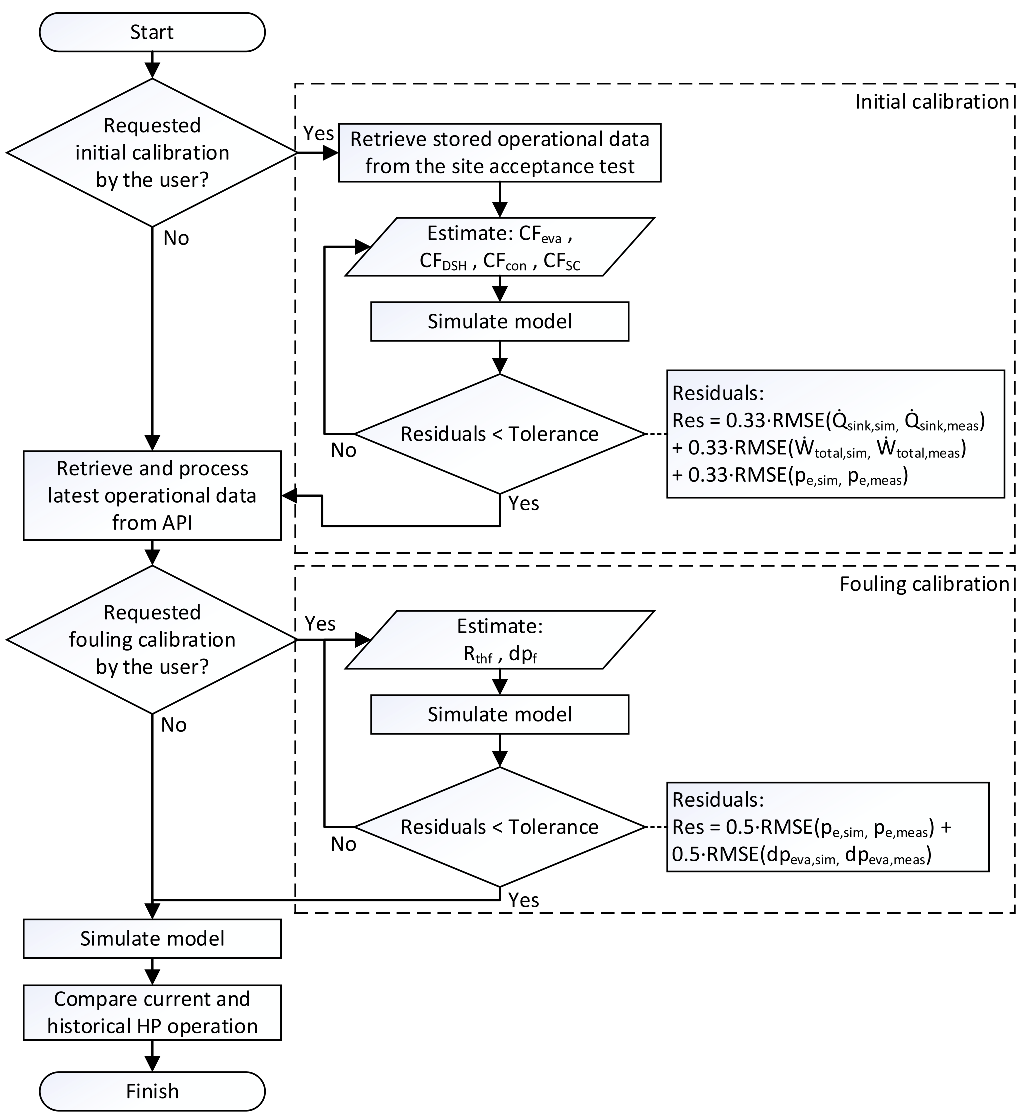

Fig. 4. Flowchart of the initial calibration and fouling calibration processes.

from a previous study [35].

2.5. Optimization of the intermediate pressure set point

Once calibrated, the adaptive and fixed models enabled the identification of an optimal $p_{m,sp}$ that maximized the COP of the heat pump. The business-as-usual value of this set point was $p_{m,sp} = 10$ bar. This value was implemented by the heat pump operator before the present study was made. The business-as-usual set point aimed at operating the high-stage compressor at full volumetric capacity, because the minimum achievable intermediate pressure was not below 12 bar. Therefore, such a set point did not necessarily lead to the optimal operation of the heat pump. Moreover, the optimal $p_{m,sp}$ was expected to be different depending on the level of fouling in the evaporator. Here, the hypothesis was that the adaptive model could allow finding the value of $p_{m,sp}$ that maximized the COP of the heat pump for different levels of fouling over time.

The optimal $p_{m,sp}$ obtained from the adaptive and fixed models were calculated through the objective function shown in Eq. (10). Here, the $p_{m,sp}$ that resulted in the maximum COP for a period n was selected as the optimal set point.

$$max\mathrm{COP}(p_{m,sp}) = \frac{\sum_{i=1}^{n} \dot{Q}_{sink,i}}{\sum_{i=1}^{n} \dot{W}_{total,i}}$$

$$s.t. p_e \leq p_{m,sp} \leq p_c \tag{10}$$

The geometric mean between the condensation and evaporation pressures shown in Eq. (11) was used as a reference value for the intermediate pressure set point in the present study. This value is commonly used as intermediate pressure in two-stage vapour compression systems and assumes equal pressure ratios for the high and low stages [36].

$$p_{m,sp,GA} = \sqrt{p_e \bullet p_c} \tag{11}$$

The adaptive model was used to calculate the optimal $p_{m,sp}$ for different levels of fouling-related thermal resistance. This enabled representing the optimal $p_{m,sp}$ as a function of p_c, p_e and the isentropic efficiencies from the high and low-stage compressors by the use of the regression model represented by Eq. (12). Here, the range in which p_e varied was defined by the range in which $R_{th,f}$ changed as a result of the fouling calibration process. The polynomial model described by Eq. (12) was referred to as the surrogate model and was adapted from the expression suggested by Tiedeman and Sherif [14] for the calculation of the optimal intermediate pressure in two-stage vapour compression refrigeration systems. The use of a surrogate model aimed at reducing the computing capacity required for determining the optimal intermediate pressure, compared to the use of the adaptive model. The surrogate model was fitted based on 70% of the dataset derived from the adaptive model, which included the optimal set point calculated based on the adaptive model for all six fouling calibration periods and the corresponding p_c, p_e, $\eta_{is,HS}$ and $\eta_{is,LS}$, that led to those optimal intermediate pressures. The remaining 30% of that dataset was used for testing the model and calculating its prediction performance represented by the coefficient of determination (R^2).

$$p_{m,sp,SM}, \Delta\mathrm{COP}, \Delta\dot{Q}_{sink} = \sum_{k=0}^{2}\sum_{j=0}^{2}\sum_{i=0}^{2} c_{i+3j+9k+1} \bullet \eta_{is,LS}^{i} \bullet \eta_{is,HS}^{i} \bullet p_e^{j} \bullet p_c^{k} \tag{12}$$

where $p_{m,sp,SM}$ is the optimal intermediate pressure calculated with the surrogate model, ΔCOP and ΔQ_{sink} are the predicted variations in the coefficient of performance and heating capacity as a result of the optimal set point, respectively, and c with the subscripts $i + 3j + 9k + 1$ are the 27 regression coefficients obtained through the fitting process. This regression model was fitted through an optimization algorithm that applied the least-squares method, available in the Python module Scikit-learn [37]. After the surrogate model was adjusted and tested, it required only the use of p_c, p_e, $\eta_{is,LS}$ and $\eta_{is,HS}$ as inputs to identify $p_{m,sp,SM}$. These inputs were obtained by the calibration of the adaptive model on the current operational data from the heat pump.

2.6. Selected operational periods for analysis

The operation of the case study heat pump was assessed based on the time intervals shown in Fig. 5. This included periods where the initial calibration, the fouling calibration (only for the adaptive model), and the CIP were used. As mentioned in Section 2.4, the initial calibration was performed based on the on-site test data obtained right after the heat pump was installed. This included 1.5 h of operation. The CIP 1 and CIP 3 shown in Fig. 5 were CIP processes applied over a three-day period with two cleaning agents, whereas the CIP 2 was applied in two days with a single cleaning agent, as described in Section 2.1. Six different operational periods were chosen for fouling calibration, which included two-hour intervals before and after each of the three CIP processes. In total, the operational periods used for fouling calibration were spread over ten calendar months, approximately.

3. Results

This section includes the main results of the present study. The results of the calibration processes are shown in Section 3.1, the estimation of the performance of the case study heat pump is presented in Section 3.2, and Section 3.3 includes the results for the optimization of the intermediate pressure set point.

3.1. Model calibration

The results from Table 4 show the parameters obtained from the initial calibration and fouling calibration. The initial calibration required significantly more iterations than the fouling calibration processes since fewer parameters were adjusted in the latter. The number of iterations was highly dependent on the algorithm and tolerances used for the minimization problem described in Section 2.4. The maximum NRMSE obtained across the different calibration processes was around 4.4%. The initial calibration results showed that the design UA-values shown in Table 2 required to be adjusted between 10% and 50% to match the model results with the operational data obtained from the on-site test of the heat pump. The fouling calibration results indicated that the fouling-related thermal resistance was between $6.3 \bullet 10^{-3}$ K/kW and $2.2 \bullet 10^{-3}$ K/kW and the source pressure drop correction factor was between 1.4 and 1. This suggested that fouling was present in all the operational periods used for fouling calibration.

3.2. Effects of fouling

The parameters obtained from the fouling calibration enabled the estimation of fouling-related effects on the evaporator thermal resistance and source pressure drop, shown in Fig. 6. Under clean conditions (light colours in Fig. 6), the thermal resistance of the evaporator had a relatively constant value of around $3 \bullet 10^{-3}$ K/kW, while the source pressure drop varied significantly across different periods as a result of the different mass flow rates in the source stream. The results indicate that the ratio between the thermal resistance due to fouling and the total thermal resistance in the evaporator ($R_{th,f}/R_{th}$) was larger than the equivalent of this ratio for the source pressure drop ($dp_{source,f}/dp_{source}$). The highest value of $R_{th,f}/R_{th}$ was around 75% (observed for calibration period 1) and did not reach a value below 45% in any of the six periods analyzed. This suggested that none of the three CIP processes applied in the heat pump was able to completely remove fouled material on the surface of the evaporator. According to the results, the three-day CIP processes (applied right after calibration periods 1 and 5) reduced the fouling-related thermal resistance between 20% and 15%, whereas they

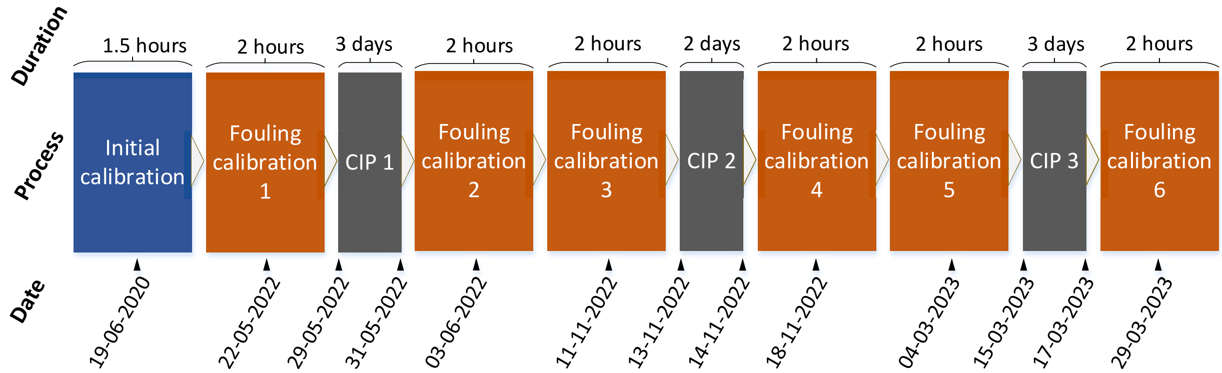

Fig. 5. Selected operational periods of the case study heat pump analyzed in the present study.

Table 4
Results from the initial calibration and fouling calibration processes.

Calibration process	Calibration parameter						Number of iterations (–)	NRMSE after calibration (%)
	CF_{DSH} (–)	CF_{con} (–)	CF_{SC} (–)	CF_{eva} (–)	$R_{th,f}$ (K/kW)	$CF_{dp,f}$ (–)		
Initial calibration	1.1	1.5	0.8	1.1	–	–	330	1.4
Fouling calibration 1 (before CIP 1)	–	–	–	–	$6.3 \bullet 10^{-3}$	1.4	93	1.8
Fouling calibration 2 (after CIP 1)	–	–	–	–	$3.1 \bullet 10^{-3}$	1.1	72	4.4
Fouling calibration 3 (before CIP 2)	–	–	–	–	$4.9 \bullet 10^{-3}$	1.4	63	3.2
Fouling calibration 4 (after CIP 2)	–	–	–	–	$3.1 \bullet 10^{-3}$	1.0	78	0.6
Fouling calibration 5 (before CIP 3)	–	–	–	–	$4.0 \bullet 10^{-3}$	1.2	87	0.8
Fouling calibration 6 (after CIP 3)	–	–	–	–	$2.2 \bullet 10^{-3}$	1.1	63	1.8

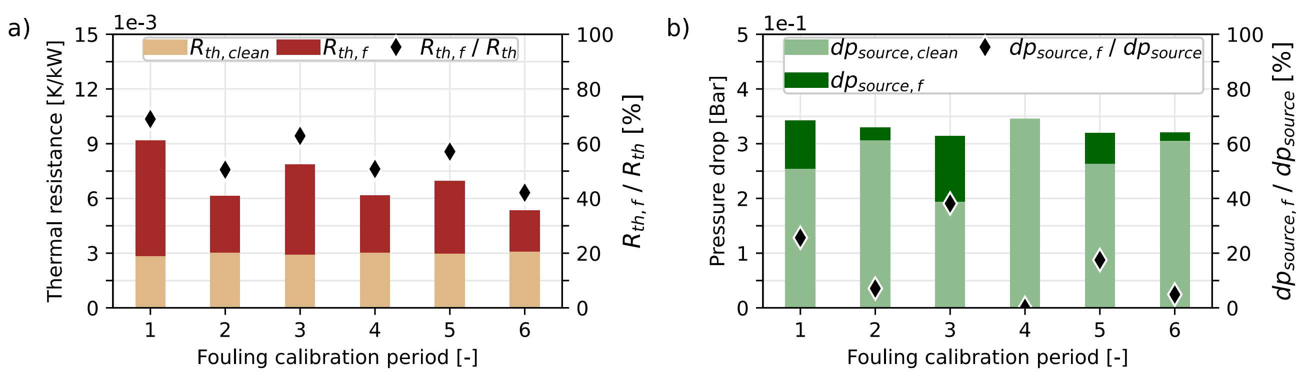

Fig. 6. Estimated effects of fouling on the evaporator thermal resistance (a) and source pressure drop (b) for the six operational periods analyzed through the fouling calibration of the model.

decreased the source pressure drop related to fouling by around 20%. The two-day CIP process (applied after calibration period 3) was observed to decrease the effects of fouling on the thermal resistance and source side pressure drop by approximately 10% and 40%, respectively.

3.3. Performance estimation

This section shows the comparison between the predicted performance of the case study heat pump using the adaptive model and fixed model.

Fig. 7 shows a box plot with the operational variables from the heat pump obtained from measurements as well as from the adaptive and fixed models. The upper and lower boundaries of each box represent the 25th and 75th percentiles of each variable, respectively. The whiskers in the plot are the maximum and minimum values of the variables, and the intermediate line in the boxes are their average values. In the initial model calibration period, the results from the adaptive and fixed models were equal. The results indicated that the adaptive and fixed models over-predicted the COP of the heat pump in periods where the heat pump did not operate close to its nominal capacity of 2 MW (i.e. fouling calibration periods 1, 2, 3, 5 and 6). The further the heat pump operated from its nominal capacity, the lower was the agreement between the simulated and measured COPs. Comparing the simulation models, the results from the adaptive model showed a better correspondence with measurements compared to those from the fixed model. The exception to this was on the heating capacity, where the estimations from the fixed model where slightly closer to measurements. The fixed model led to larger overestimations of the evaporation pressure and thereby the COP, as well as underestimations of the source pressure drop. This mismatch was greater in periods with higher values of fouling-related thermal resistance (see Table 4), namely the fouling calibration periods 1, 3 and 5.

Fig. 8 shows the residuals between simulated and measured variables, where a single residual value in the box plots represented the relative difference between measurements and simulations for each point in time. These results include the difference between the mean values of the residuals obtained from the adaptive and fixed models. The same residuals from both models were obtained in the initial calibration

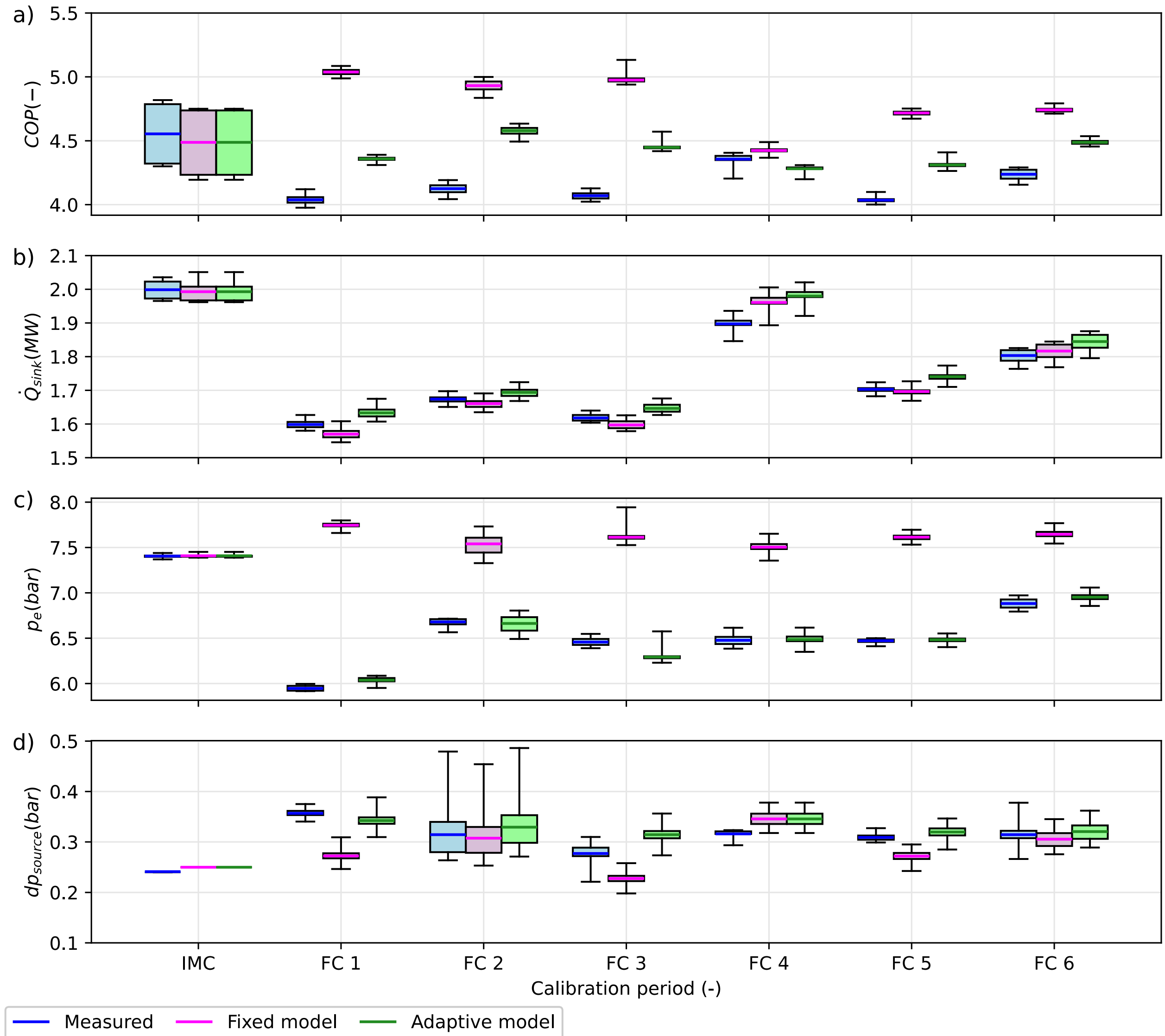

Fig. 7. Measured and simulated operational variables obtained from the adaptive and fixed models. IMC: Initial model calibration; FC: Fouling calibration.

period. In the fouling calibration periods, the adaptive model estimated more accurately the COP and less accurately the heating capacity compared to the fixed model. The residuals related to the simulated values of the COP, heat capacity, and evaporation pressure from the adaptive model were within ±15%, ±5%, and ± 5%, respectively. This variability was larger for the source pressure drop residuals (between −35% and 18%), which was likely to be caused by variations in the source mass flow rate that were not included in the regression model to determine the source pressure drop, described in Section 2.3. The largest difference between the results from adaptive and fixed models occurred in the fouling calibration period 1, where the adaptive model provided estimates of the COP that were around 17% closer to measurements than those from the fixed model. This was mainly attributed to the calibration of the fouling-related thermal resistance, which led to simulated values of the evaporation pressure that were nearly 30% closer to measurements by the use of the fouling calibration process rather than only using the initial calibration.

3.4. Set point optimization

A detailed representation of the relationship between the intermediate pressure set point and the COP of the heat pump in the different operational periods is presented in Fig. 12, included in Appendix B. Fig. 9 shows the influence of the intermediate pressure set point on the COP and heat capacity for different levels of thermal resistance due to fouling. This includes fouling calibration periods 1, 4 and 5, where the heat pump operated with heat capacities of around 1.5 MW, 1.8 MW and 1.6 MW, respectively. Here, the fouling-related thermal resistance was varied between zero and the maximum value obtained from the operational periods used for fouling calibration (see Table 4). The results in Fig. 9 indicated that higher fouling levels lowered the optimal intermediate pressure set point. This, in turn, reduced the performance improvement and heat capacity reduction associated with that optimal set point. As seen in Fig. 9, the optimal intermediate pressure set point led to a COP increase of up to 3%, which was calculated for a thermal resistance due to fouling equal to zero. The results shown in Fig. 9 were applied to calculate the fitting coefficients from the surrogate model. These coefficients together with the results from the surrogate model across different evaporation pressures are shown in Table 5 and Fig. 13, respectively, located in Appendix C.

A comparison was made between the optimal intermediate pressure set point obtained from the geometric average, fixed model, adaptive model and surrogate model for the six fouling calibration periods, as shown in Fig. 10. The optimal intermediate pressure set point led to a

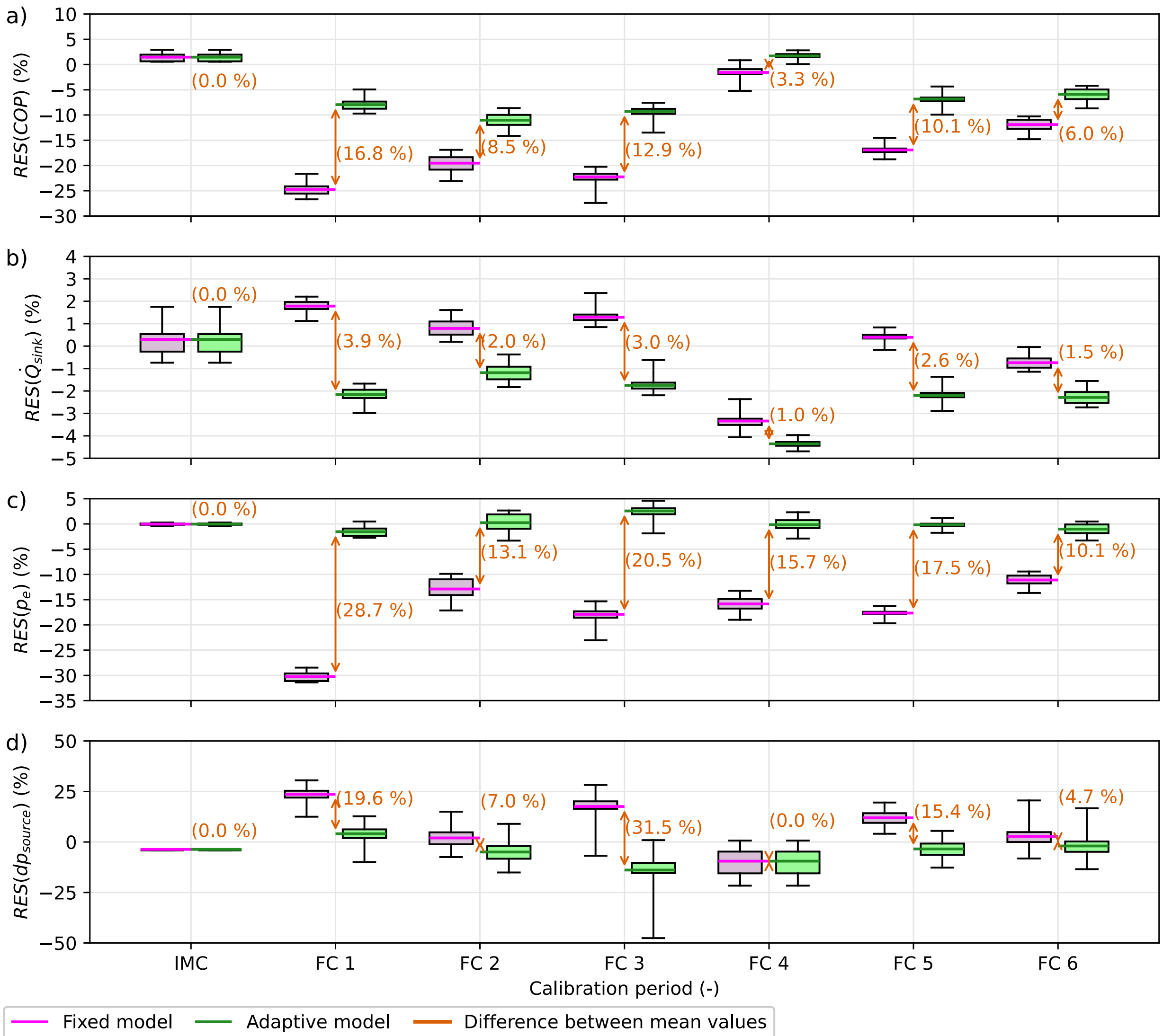

Fig. 8. Residuals of the simulated variables obtained through the adaptive and fixed models. IMC: Initial model calibration; FC: Fouling calibration.

larger increase in COP than a decrease in the heat capacity for all the levels of fouling and heat capacities analyzed. All the model-based approaches proposed in the present study led to similar estimations of the optimal intermediate pressure set point. These were between 1.3 bar and 2 bar higher than the set points derived from the geometric average and led to improvements of the COP that were within 0.2% and 1.3% above this average value. The fixed model led to an overestimation of the COP improvement and heat capacity reduction as a result of such optimal set point, compared to the other model-based approaches, particularly in periods where the heat pump operated at higher heat capacities (i.e. fouling calibration periods 4, 5 and 6). The estimations from the surrogate model were similar to those from the adaptive model in terms of optimal set points as well as their related COP and heat capacity variations. Here, the largest difference was found in periods in which the heat pump operated at the lowest heat capacities, namely fouling calibrations periods 1 and 3.

4. Discussion

The correspondence between simulated and measured operational variables from the case study heat pump increased when the adaptive model was used instead of the fixed model (see Fig. 7 and Fig. 8). The difference between the NRMSE obtained from the adaptive and fixed models were between 3.3 and 16.8 percentage points for the COP, and between 1 and 3.9 percentage points for the heat capacity, where the largest difference occurred in the period with the highest estimated levels of fouling (see Table 4). The adaptive model showed that fouling had a larger impact on the evaporator thermal resistance than on the source pressure drop. This model also enabled the comparison between different CIP processes regarding the degree to which they were able to mitigate the fouling-related effects on the evaporator.

The use of an adaptive model-based framework represents an alternative to the use of dedicated sensing devices for fouling characterization, which are described in Bott [7]. Such a framework provides a remote assessment of fouling-related effects, takes advantage of existing sensing devices, and does not require the mechanical intervention of the heat pump. This was particularly beneficial for the heat pump assessed in the present study, in which the evaporator could not be dismantled for cleaning purposes and sufficient sensing devices for the development and calibration of the quasi-steady-state model were already present in the heat pump. However, the inclusion of additional measurement points to develop and validate the adaptive model such as refrigerant mass flow rates and subcooling temperature difference would have allowed to increase the correspondence between the simulation results and measurements as well as extending the reusability of the model.

The proposed framework offers the possibility to characterize other

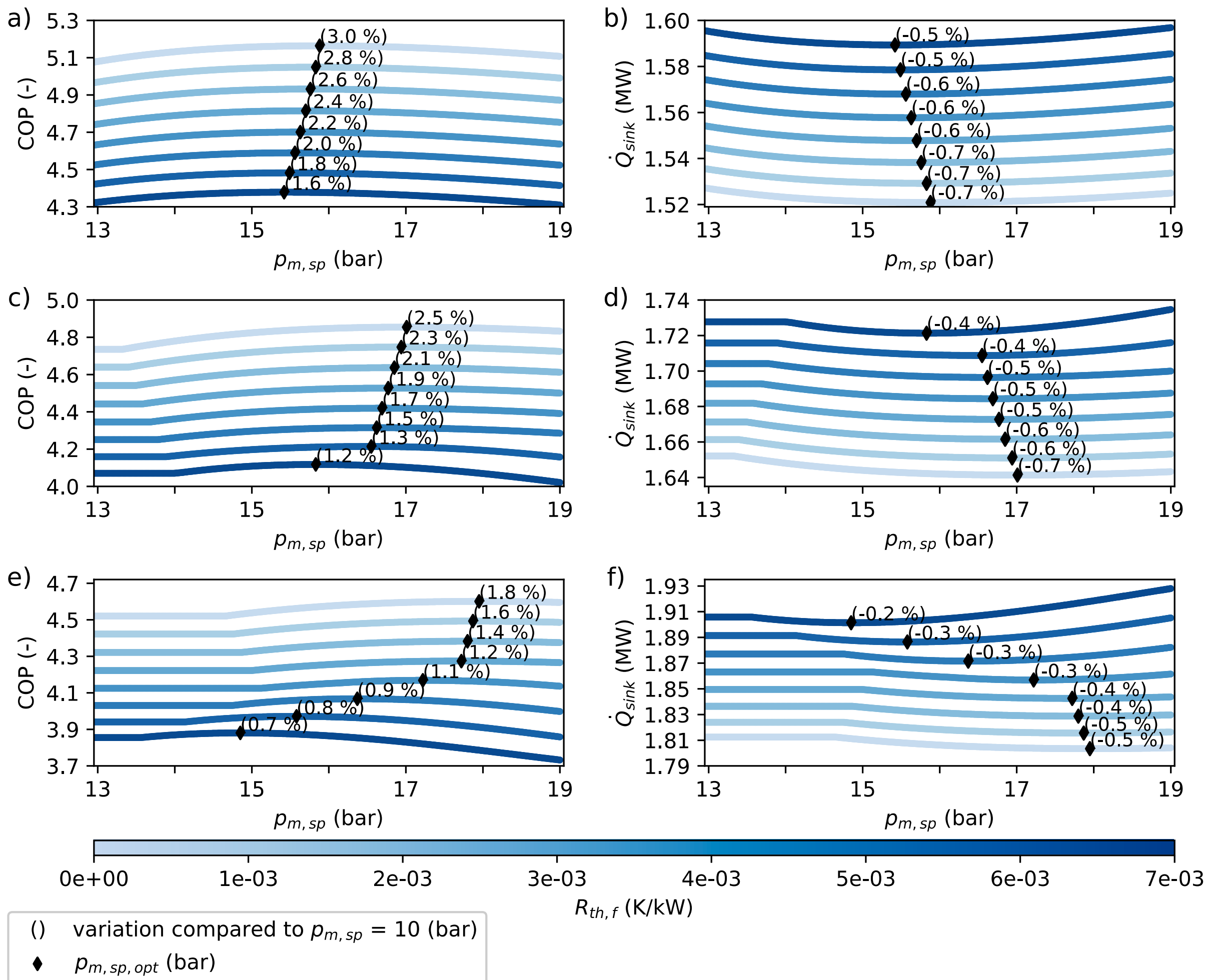

Fig. 9. Effect of fouling-related thermal resistance on the optimal intermediate pressure set point, as well as the resulting changes in COP and heat capacity. This analysis covers fouling calibration periods 1 (shown in a) and b)), 5 (shown in c) and d)), and 4 (shown in e) and f)), each corresponding to different heat capacities provided by the heat pump during operation.

phenomena than fouling that leads to gradual performance degradation. One example of this could be the aging of components, where parameters related to the aging process could be represented in a model and calibrated online based on measurements. In this example, the selection of the calibration parameters related to the aging processes may impose a challenge. As described in [38], component aging in vapour compression systems can depend on numerous and unrelated elements that can be difficult to represent. Unlike component aging, the effects of fouling on the thermal resistance and pressure drop in the source side of heat pumps are described in multiple experimental studies [39–41]. In such studies, the amount of fouled material and its composition were measured and characterized, but in the heat pump analyzed in the present study the industrial waste water used as heat source had an unknown chemical composition that was expected to vary over time. Here, the use of the fouling-related thermal resistance and source pressure drop enabled the characterization of the performance degradation due to fouling regardless of the impossibility of providing a detailed description of the fouling mechanisms present in the heat pump.

Fouling was observed to affect the optimal value for the intermediate pressure set point as well as the COP increase and heat capacity reduction related to that set point. This suggests that the characterization of the fouling-related thermal resistance is beneficial for the adjustment of the intermediate pressure set point. Not accounting for the variation of fouling levels over time and thereby using a model calibrated only once led to the overestimation of the changes in the COP and heat capacity related to the optimal intermediate pressure set point, as shown in Fig. 10.

The results from Fig. 10 highlighted the importance of including estimations of compressor isentropic efficiencies for optimizing intermediate pressures in two-stage vapour compression systems, which was also indicated in previous studies [14,42,43]. The optimal intermediate pressure set points obtained from the adaptive model were between 7% and 10% above the geometric average results (seen in Fig. 10). Tiedeman et al. [14] also found that the optimal intermediate pressure in a two-stage vapour compression system with ammonia was above the geometric average value. This discrepancy was up to 26% for ideal compressors and was even higher for isentropic efficiencies below 100%. The optimal intermediate pressure estimations in the present study are expected to be closer to optimal values derived from measurements than those from Tiedeman et al. Unlike the present study, Tiedeman et al. did not account for the volumetric efficiencies of the compressors and assumed equal isentropic efficiencies for the high and low stage compressors. Moreover, the surrogate model used in the present study led to estimations of the COP related to the optimal intermediate pressure set point that were within 0.5% compared to the adaptive model results. This error was lower compared to the results derived from polynomial model from Tiedeman et al., which exhibited a 2% deviation with the optimal COP values.

The residuals shown in Fig. 8 were larger than the maximum COP

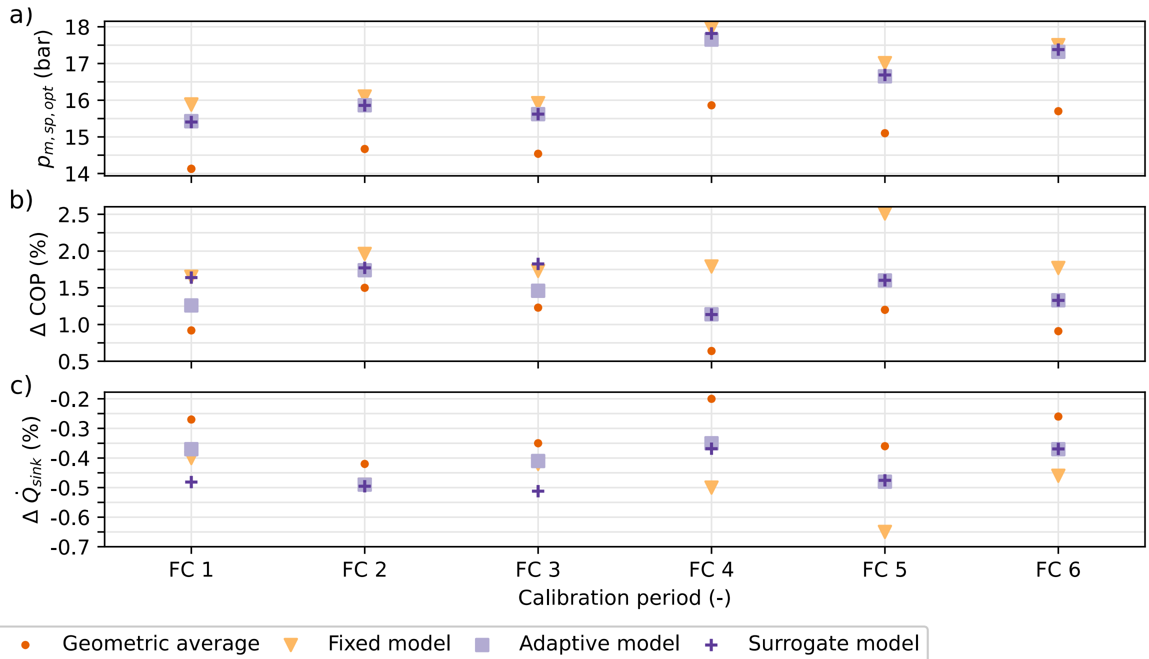

Fig. 10. Comparison between the optimal intermediate pressure set points obtained from different approaches as well as the COP and heat capacity variations derived from those set points.

improvement related to the optimal intermediate pressure set point of around 3%, seen in Fig. 9. The results derived from the adaptive model and the surrogate model may differ when tested on different vapour compression systems or in the actual case study heat pump. Previous studies done by Wang et al. [15] and Gong et al. [16] adjusted intermediate pressure set points based on changing boundary conditions in two-stage vapour compression systems, improving the COP compared to using fixed set points by 5% and 8%, respectively. These results were obtained from the implementation of extremum seeking control strategies in simulation models, which are expected to be different obtained under real-world operational conditions. Nonetheless, the findings from Wang et al., Gong et al. and the present study underscore the potential energy performance enhancements derived from adjusting the intermediate pressure set point accounting for varying boundary conditions in two-stage vapour compression systems.

External factors leading to discrepancies between measured and simulated variables, and not included in the calibration process were lumped into the calibration parameters. In the present study, such factors may have included the use of constant heat transfer coefficients in the heat exchangers, the presence of non-condensables in the refrigerant, and the fouling of oil on the refrigerant side of the evaporator. However, these factors were not likely to change significantly between the periods used for fouling calibration, as a result, they did not prevent the relative comparison between the effects of fouling on the different operational intervals assessed in this study. This emphasizes the importance of considering all relevant parameters with time-varying impacts on variables utilized as targets for online model calibration.

It is expected that less time will be required for the development and implementation of the fixed model compared to the adaptive model and its surrogate model in different heat pumps. The adaptive model requires a data infrastructure that enables the retrieval and processing of operational data in real-time, besides the heat pump design information also used to build and calibrate the fixed model. The possibility to represent the heat pump operation in real-time may be useful for monitoring faster phenomena than fouling such as defective compressor components. The development of the surrogate model will take longer than that of the adaptive model due to its dependence on the results from the online calibration of the adaptive model based on retrieved operational data. Once developed, the surrogate model will produce similar estimations to the adaptive model for optimal intermediate pressure set points, but more rapidly because there is no requirement for an optimization routine. This may enable the use of the surrogate model in component or system controllers.

The NRMSE and number of iterations obtained from the initial calibration and fouling calibration (see Table 4) as well as the residuals between simulation and measured results (see Fig. 8) were affected by key elements related to the calibration methods included in this study. These included the size and variability of the operational data used for calibration, the optimization algorithm used for error minimization, the calibration parameters, the calibration targets and their corresponding weights. The selection of these elements was a result of an iterative process involving testing and refinement. In this context, data-driven techniques can contribute to defining specific aspects of the calibration process and minimize the use of heuristics. For example, parameter selection can be aided by the use of sensitivity analysis methods, as shown in a related study [24]. Similarly, operational periods utilized for calibration could be determined using thresholds or pattern recognition techniques. These approaches could identify time intervals where calibration will significantly improve the correspondence between simulated and measured data. Despite the potential to automatize the proposed calibration methods, it is likely that human intervention will remain essential for the development, interpretation and validation of such methods.

5. Conclusions

The present study assessed the applicability of a novel framework that aimed at enhancing the energy performance of a large-scale heat pump in operation. This was done by determining optimal intermediate pressure set points for the heat pump exposed to different levels of performance degradation due to fouling. The framework was based on the real-time adaptation of digital twins, where a simulation model was calibrated based on operational data from the heat pump. An online calibration method adjusted fouling-related parameters in the simulation model, which was performed after an initial calibration of time-independent design parameters. The results demonstrated that the online calibration reduced the simulation errors compared to the initial calibration alone between 3 and 17 percentage points for the COP, and between 1 and 4 percentage points for the heat capacity. The online calibration also enabled estimating the influence of fouling on evaporator thermal resistance and source pressure drop, and assessing the effect of cleaning-in-place processes on fouling mitigation. Moreover, the model calibrated online and a surrogate model derived from it were applied for the estimation of an optimal intermediate pressure set point. This set point enhanced the COP of the heat pump by up to 3%, which was influenced by varying fouling levels. The results underscored the potential of the proposed framework for improving the energy performance of large-scale heat pumps operating under real-world conditions.

CRediT authorship contribution statement

José Joaquín Aguilera: Writing – review & editing, Writing – original draft, Visualization, Validation, Software, Resources, Methodology, Investigation, Formal analysis, Data curation, Conceptualization. **Wiebke Meesenburg:** Writing – review & editing, Visualization, Supervision, Formal analysis, Conceptualization. **Wiebke Brix Markussen:** Writing – review & editing, Validation, Supervision, Formal analysis. **Benjamin Zühlsdorf:** Writing – review & editing, Supervision, Resources, Funding acquisition. **Brian Elmegaard:** Writing – review & editing, Supervision, Project administration, Funding acquisition.

Declaration of competing interest

The authors declare that they have no known competing financial interests or personal relationships that could have appeared to influence the work reported in this paper.

Data availability

The authors do not have permission to share data.

Acknowledgements

This work was funded by EUDP (Energy Technology Development and Demonstration) under the project "Digital twins for large-scale heat pump and refrigeration systems" (project number: 64019-0570).

Appendix A. Example of operational data used in the present study

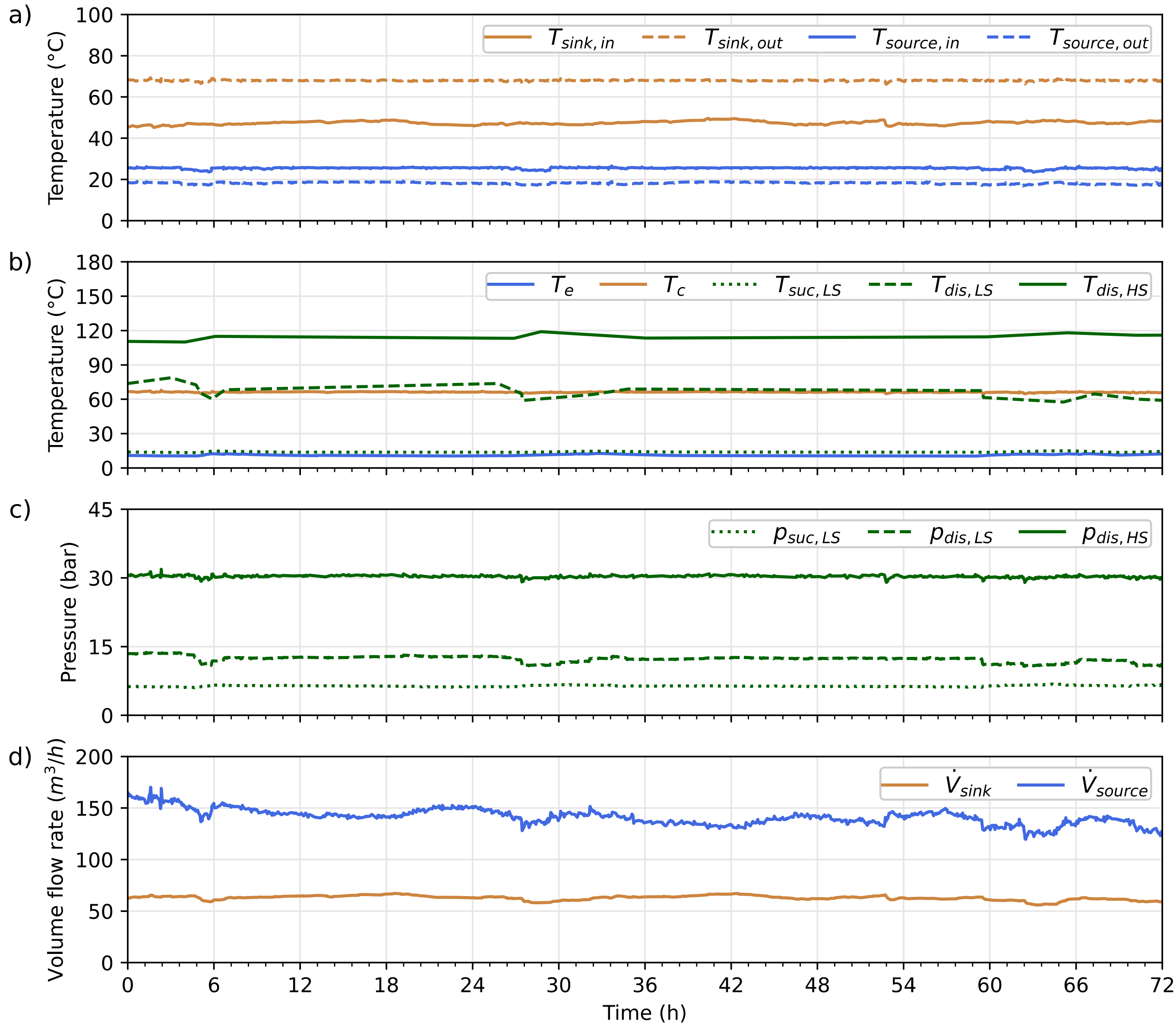

Fig. 11. Example of the operational data of the heat pump retrieved from the SCADA server.

Appendix B. Relationship between intermediate pressure set point and COP

Fig. 12 shows the influence of the intermediate pressure set point on the mean COP and mean heat capacity obtained from the adaptive model and fixed model. Each of the fouling calibration periods showed a global optimal solution, where an optimal intermediate pressure set point led to the maximum increase of the COP and a reduction of the heat capacity. Fig. 12 indicated that that the optimal intermediate pressure set point before the use of the CIP processes was lower than after their implementation. This was expected because fouling often leads to a reduction of the evaporation pressure, decreasing the average value between the condensation and evaporation pressures, which is often used as an approximation of the optimal intermediate pressure.

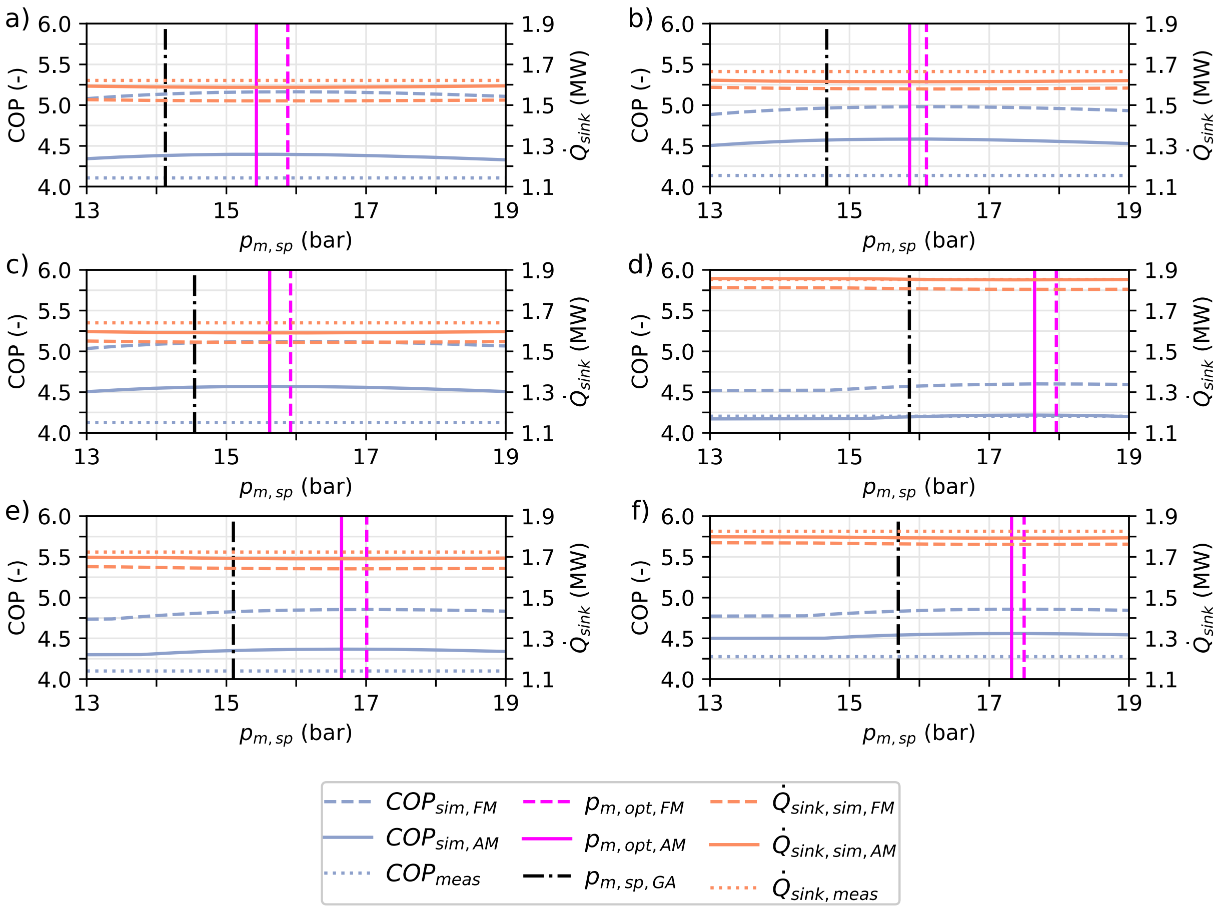

Fig. 12. Effect of the intermediate pressure set point on the mean COP and mean heat capacity of the heat pump over each of the six periods selected for fouling calibration (i.e. a) to f)). FM: fixed model; AM: adaptive model; GA: geometric average.

Appendix C. Surrogate model

The results from Fig. 9 were applied for the adjustment and testing of the surrogate model represented by Eq. (12). The regression coefficients as well as the coefficients of determination related to the surrogate model are presented in Table 5. The coefficients of determination indicated that the surrogate model was suitable for the estimation of the intermediate pressure set point ($R^2 = 99.4\%$), COP variation ($R^2 = 99.9\%$), and heat capacity variation ($R^2 = 99.9\%$). This surrogate model was highly dependent on the polynomials that described the isentropic and volumetric efficiencies of the compressors, presented in Section 2.3.

Table 5
Regression results obtained from the fitting process of the surrogate model.

Predicted variable	$p_{m,sp,SM}$	ΔCOP	ΔQ_{sink}
R2 (%)	99.4	99.9	99.9
c1 (–)	22,569,921.4	850,978.9	−229,713.7
c2 (–)	−1,334,680.0	−45,511.5	14,658.8
c3 (–)	−14,351,500.0	−358,926.0	315,153.0
c4 (–)	19,715.3	605.7	−229.5
c5 (–)	1,143,860.0	27,458.0	−24,241.2
c6 (–)	841,265.0	20,515.6	−18,606.5
c7 (–)	−12,305.0	−292.9	274.1
c8 (–)	−67,080.5	−1594.2	1425.3
c9 (–)	981.2	23.1	−20.9
c10 (–)	4,757,840.0	155,142.0	−64,939.4
c11 (–)	46,634,500.0	1,154,650.0	−1,039,050.0
c12 (–)	−70,060.7	−2092.8	994.2
c13 (–)	−3,609,400.0	−86,558.6	76,358.1
c14 (–)	−2,732,380.0	−66,230.9	61,270.7
c15 (–)	39,946.3	948.9	−901.6
c16 (–)	211,671.0	5034.2	−4488.8
c17 (–)	−3096.2	−73.1	65.9
c18 (–)	−80,700,600.0	−2,866,920.0	1,048,260.0
c19 (–)	70,200,100.0	2,384,660.0	−1,044,590.0

(continued on next page)

Table 5 (*continued*)

Predicted variable	$p_{m,sp,SM}$	ΔCOP	ΔQ_{sink}
c20 (−)	−4,130,030.0	−130,248.0	63,800.5
c21 (−)	−37,571,700.0	−923,020.0	844,091.0
c22 (−)	60,681.6	1775.2	−966.0
c23 (−)	2,827,060.0	67,907.1	−59,360.2
c24 (−)	2,200,700.0	53,103.5	−49,732.5
c25 (−)	−32,162.2	−763.2	731.3
c26 (−)	−165,814.0	−3954.9	3489.8
c27 (−)	2425.6	57.5	−51.2

The results from the surrogate model regarding the optimal intermediate pressure set point as well as the change in the COP and heat capacity derived from such a set point, are shown in Fig. 13. The results revealed that, at a fixed condensation pressure, fouling influenced the evaporation pressure, causing a shift in the optimal intermediate pressure set point between 3 bar (at $p_c = 38.5$ bar) and 0.4 bar (at $p_c = 33.1$ bar). The results also showed that higher fouling levels reduced the COP increase related to the optimal intermediate pressure set point between 1.4% and 1.1%.

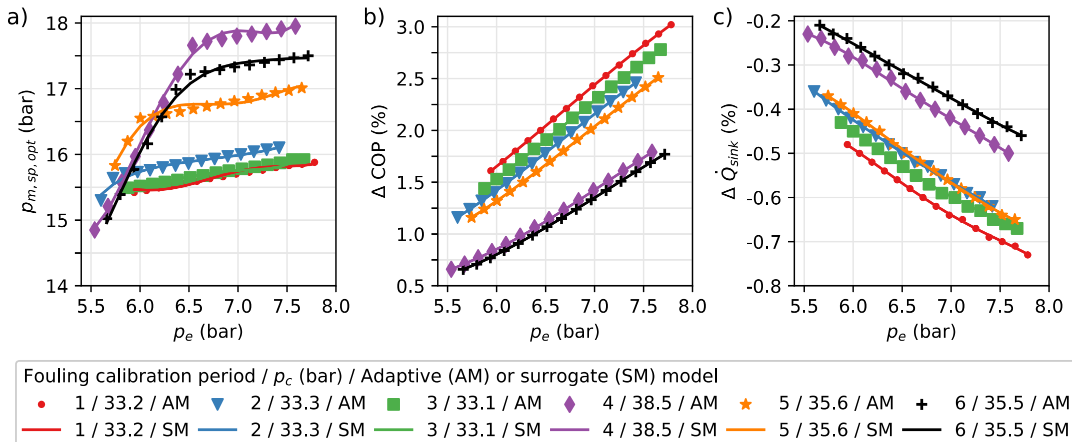

Fig. 13. Predicted optimal intermediate pressure set point by the surrogate model as well as the resulting variations on the COP and heat capacity. SM: surrogate model; AM: adaptive model.

References

[1] IEA. The future of heat pumps. Paris, France. [Online]. Available: https://www.iea.org/reports/the-future-of-heat-pumps; 2022.
[2] David A, Mathiesen BV, Averfalk H, Werner S, Lund H. Heat roadmap Europe: large-scale electric heat pumps in district heating systems. Energies 2017;10(4):1–18. https://doi.org/10.3390/en10040578.
[3] Schlosser F, Jesper M, Vogelsang J, Walmsley TG, Arpagaus C, Hesselbach J. Large-scale heat pumps: applications, performance, economic feasibility and industrial integration. Renew Sustain Energy Rev Nov 2020;133:110219. https://doi.org/10.1016/j.rser.2020.110219.
[4] Energistyrelsen [Danish Energy Agency]. Klimastatus og –fremskrivning 2022 (KF22): El og fjernvarme (ekskl. affaldsforbrænding) [Climate status and projection 2022 (KF22): Electricity and district heating (excluding waste incineration)]. Copenhagen, Denmark. 2022.
[5] PlanEnergi. Heatpumpdata.eu: Large-scale heat pumps in Danish district heating systems. https://heatpumpdata.eu/; 2024 [accessed 24 February 2024].
[6] Aguilera JJ, Meesenburg W, Ommen T, Markussen WB, Poulsen JL, Zühlsdorf B, et al. A review of common faults in large-scale heat pumps. Renew Sustain Energy Rev Oct 2022;168:112826. https://doi.org/10.1016/J.RSER.2022.112826.
[7] Bott TR. Fouling of heat exchangers. Amsterdam, The Netherlands: Elsevier Science B.V; 1995. https://doi.org/10.1016/B978-0-444-82186-7.X5000-3.
[8] Pogiatzis T, Ishiyama EM, Paterson WR, Vassiliadis VS, Wilson DI. Identifying optimal cleaning cycles for heat exchangers subject to fouling and ageing. Appl Energy Jan 2012;89(1):60–6. https://doi.org/10.1016/J.APENERGY.2011.01.063.
[9] Brahim F, Augustin W, Bohnet M. Numerical simulation of the fouling process. Int J Therm Sci Mar 2003;42(3):323–34. https://doi.org/10.1016/S1290-0729(02)00021-2.
[10] Pelet X, Favrat D. Performances of 3.9 MWth Ammonia heat pumps within a district heating cogeneration power plant status after eleven years of operation. In: Conférence de l'Annex 22 de l'IEA, Gatlinburg, Tennessee, USA; 1997. no. 195124.
[11] Gjengedal S, Stenvik LA, Ramstad RK, Ulfsnes JI, Hilmo BO, Frengstad BS. Online remote-controlled and cost-effective fouling and clogging surveillance of a groundwater heat pump system a case study from Lena terrace in Melhus, Norway. Bull Eng Geol Environ 2021;80:1063–72. https://doi.org/10.1007/s10064-020-01963-z.
[12] Borges S, Jöhnk L, Klebig T, Vering C, Müller D. Fault detection and diagnosis by machine learning methods in air-to-water heat pumps: Evaluation of evaporator fouling. In: *Proceedings of ECOS 2023: 36th International Conference on Efficiency, Cost, Optimization, Simulation and Environmental Impact of Energy Systems*; 2023. p. 815–26.
[13] Meesenburg W, Aguilera JJ, Kofler R, Markussen WB, Elmegaard B. Prediction of fouling in sewage water heat pump for predictive maintenance. In: *Proceedings of ECOS* 2022: 35th international conference on efficiency, Cost, Optimization, Simulation and Environmental Impact of Energy Systems; 2022. p. 12.
[14] Tiedeman JS, Sherif SA. Optimum coefficient of performance and exergetic efficiency of a two-stage vapour compression refrigeration system Sep 2003;217(9):1027–38. https://doi.org/10.1243/095440603322407263.
[15] Wang W, Zhou Q, Tian G, Hu B, Li Y, Cao F. The intermediate temperature optimization for cascade refrigeration system and air source heat pump via extreme seeking control. Int J Refrig Sep 2020;117:150–62. https://doi.org/10.1016/j.ijrefrig.2020.05.007.
[16] Gong Y, Liu G, Lu Z. Extremum seeking control for real-time optimization of high temperature heat pump systems incorporating vapor injection. Therm Sci Eng Prog Jul 2023;42:101867. https://doi.org/10.1016/J.TSEP.2023.101867.
[17] Kritzinger W, Karner M, Traar G, Henjes J, Sihn W. Digital twin in manufacturing: a categorical literature review and classification. IFAC-PapersOnLine Jan 2018;51(11):1016–22. https://doi.org/10.1016/J.IFACOL.2018.08.474.
[18] Ma S, Ding W, Liu Y, Ren S, Yang H. Digital twin and big data-driven sustainable smart manufacturing based on information management systems for energy-intensive industries. Appl Energy Nov 2022;326:119986. https://doi.org/10.1016/J.APENERGY.2022.119986.
[19] Liu M, Fang S, Dong H, Xu C. Review of digital twin about concepts, technologies, and industrial applications. J Manuf Syst 2020;(October 2019):1–16. https://doi.org/10.1016/j.jmsy.2020.06.017.
[20] Song Y, Xia M, Chen Q, Chen F. A data-model fusion dispatch strategy for the building energy flexibility based on the digital twin. Appl Energy Feb 2023;332:120496. https://doi.org/10.1016/J.APENERGY.2022.120496.
[21] Machado DO, Chicaiza WD, Escaño JM, Gallego AJ, de Andrade GA, Normey-Rico JE, et al. Digital twin of a Fresnel solar collector for solar cooling. Appl Energy Jun 2023;339:120944. https://doi.org/10.1016/J.APENERGY.2023.120944.
[22] Spinti JP, Smith PJ, Smith ST, Díaz-Ibarra OH. Atikokan digital twin, Part B: Bayesian decision theory for process optimization in a biomass energy system. Appl Energy Mar 2023;334:120625. https://doi.org/10.1016/J.APENERGY.2022.120625.
[23] You M, Wang Q, Sun H, Castro I, Jiang J. Digital twins based day-ahead integrated energy system scheduling under load and renewable energy uncertainties. Appl

Energy Jan 2022;305:117899. https://doi.org/10.1016/J.APENERGY.2021.117899.
[24] Vering C, Borges S, Coakley D, Krützfeldt H, Mehrfeld P, Müller D. Digital twin design with on-line calibration for HVAC systems in buildings. 2021.
[25] Klingebiel J, Salamon M, Bogdanov P, Venzik V, Vering C, Müller D. Towards maximum efficiency in heat pump operation: self-optimizing defrost initiation control using deep reinforcement learning. Energ Buildings Jul 2023:113397. https://doi.org/10.1016/J.ENBUILD.2023.113397.
[26] Chen WD, Hasanien HM, Chua KJ. Towards a digital twin approach – experimental analysis and energy optimization of a multi-bed adsorption system. Energ Conver Manage Nov 2022;271:116346. https://doi.org/10.1016/J.ENCONMAN.2022.116346.
[27] Zhang K, Wu Q, Li H, Zhang R, Li J, Jiang F, et al. Intelligent optimal control strategy of heat pump system based on digital twins. J Phys Conf Ser 2023;2452(1):12029. https://doi.org/10.1088/1742-6596/2452/1/012029.
[28] Huang ZF, Soh KY, Islam MR, Chua KJ. Digital twin driven life-cycle operation optimization for combined cooling heating and power-cold energy recovery (CCHP-CER) system. Appl Energy Oct 2022;324:119774. https://doi.org/10.1016/J.APENERGY.2022.119774.
[29] Aguilera JJ, Meesenburg W, Ommen T, Poulsen JL, Kramer KR, Markussen WB, et al. Operational challenges in large-scale ammonia heat pump systems. In: *Proceedings of ECOS* 2021: 34th international conference on efficiency, Cost, Optimization, Simulation and Environmental Impact of Energy Systems; 2021. p. 12.
[30] Church P, Mueller H, Ryan C, Gogouvitis SV, Goscinski A, Haitof H, et al. SCADA Systems in the Cloud. In: Zomaya AY, Sakr S, editors. Handbook of Big Data technologies. Cham: Springer International Publishing; 2017. p. 691–718. https://doi.org/10.1007/978-3-319-49340-4_20.
[31] Bell IH, Wronski J, Quoilin S, Lemort V. Pure and pseudo-pure fluid thermophysical property evaluation and the open-source thermophysical property library CoolProp. 2014. https://doi.org/10.1021/ie4033999.
[32] Virtanen P, Gommers R, Oliphant TE, Haberland M, Reddy T, Cournapeau D, et al. SciPy 1.8.0: fundamental algorithms for scientific computing in Python. Nat Methods 2020;17(3):261–72. https://doi.org/10.1038/s41592-019-0686-2.
[33] Paterson WR. A replacement for the logarithmic mean. Chem Eng Sci 1984;39(11):1635–6. https://doi.org/10.1016/0009-2509(84)80090-1.
[34] Trucano TG, Swiler LP, Igusa T, Oberkampf WL, Pilch M. Calibration, validation, and sensitivity analysis: what's what. Reliab Eng Syst Saf Oct 2006;91(10–11):1331–57. https://doi.org/10.1016/J.RESS.2005.11.031.
[35] Aguilera JJ, Meesenburg W, Markussen WB, Zühlsdorf B, Elmegaard B. Online model-based framework for operation and fouling monitoring in a large-scale heat pump. In: *Proceedings of ECOS 2023: 36th International Conference on Efficiency,* Cost, Optimization, Simulation and Environmental Impact of Energy Systems; 2023. p. 3296–306.
[36] Torrella E, Llopis R, Cabello R. Experimental evaluation of the inter-stage conditions of a two-stage refrigeration cycle using a compound compressor. Int J Refrig Mar 2009;32(2):307–15. https://doi.org/10.1016/J.IJREFRIG.2008.05.006.
[37] Pedregosa F, Varoquaux G, Gramfort V Michel, Thirion B, Grisel O, Blondel M, et al. Scikit-learn: machine learning in Python. J Mach Learn Res 2011;12:2825–30.
[38] Blahnik DE, Camp TW. Aging assessment of essential HVAC chillers used in nuclear power plants. Richland, Washington, U.S.A: Pacific Northwest National Laboratory; 1996. Accessed: Aug. 11, 2023. [Online]. Available: https://inis.iaea.org/search/search.aspx?orig_q=RN:28037419.
[39] Yoon SH, Payne WV, Domanski PA. Residential heat pump heating performance with single faults imposed. Appl Therm Eng 2011;31(5):765–71. https://doi.org/10.1016/j.applthermaleng.2010.10.023.
[40] Shen C, Yang L, Wang X, Jiang Y, Yao Y. An experimental and numerical study of a de-fouling evaporator used in a wastewater source heat pump. Appl Therm Eng Sep 2014;70(1):501–9. https://doi.org/10.1016/j.applthermaleng.2014.05.055.
[41] Seol SH, Serageldin AA, Kwon OK. Experimental research on a heat pump applying a ball-circulating type automatic fouling cleaning system for fish farms. Energies Nov 2020;13(22):5856. https://doi.org/10.3390/EN13225856.
[42] Hartmund Jørgensen P, Ommen T, Elmegaard B. Quantification and comparison of COP improvement approaches for large-scale ammonia heat pump systems. Int J Refrig Sep 2021;129:301–16. https://doi.org/10.1016/J.IJREFRIG.2021.04.016.
[43] Jiang S, Wang S, Jin X, Yu Y. The role of optimum intermediate pressure in the design of two-stage vapor compression systems: a further investigation. Int J Refrig Oct 2016;70:57–70. https://doi.org/10.1016/J.IJREFRIG.2016.06.024.